Acta Mech 224, 1397–1414 (2013)
DOI 10.1007/s00707-013-0812-7

Peng Li · Feng Jin

The anti-plane vibration of a quartz plate with an additional partial non-uniform mass layer for acoustic wave sensing

Received: 25 September 2012 / Revised: 1 January 2013 / Published online: 3 February 2013

Abstract The anti-plane vibration of a quartz plate having an additional partial non-uniform mass layer is solved by ignoring the effect of small c_{56} in comparison with other elastic constants. This analysis is based on the trigonometric series solution, and the convergence is examined. Numerical simulation is conducted for several different types of layers of different thicknesses using linear, cosine, and quadratic functions. The frequency spectrums, in addition to the length and mass fraction of the layer, are discussed separately. Compared with the homogeneous mass layer, the non-homogeneous layer with greater inertia leads to earlier appearance of the higher modes and more modes trapped under the same condition. Especially, there is no energy trapping in the plate with a fully covered uniform mass layer. However, this kind of energy trapping can be obtained again when the surface is non-uniform for some cases.

1 Introduction

Frequency shifts in a crystal resonator or mass sensor that occurs due to a thin mass layer added to its surface is an important issue in frequency stability analysis of crystal resonators used for time-keeping, telecommunication, and sensing [1,2]. When a thin layer of another material is added to the surface of a resonator, the resonant frequencies become lower; that this primarily occurs because of the inertia of the mass layer is the simplest explanation (Sauerbery's equation) [3]. This effect has been used to make mass sensors for measuring the density and thickness of the layer [4]. For instance, quartz crystal microbalance (QCM) is used to detect the micro-mass changes and physical properties of thin layers deposited on crystal surfaces [5,6], which have important applications in chemical and biological sensing devices.

Due to its wide application, the study of the mechanism of operation of quartz crystal devices has drawn increasing attention from researchers in recent years [7]. The dissipation effects of an electroded AT-cut quartz resonator due to the intrinsic damping of the quartz plate and the surface damping of the coated electrodes were discussed by Lu et al. [8]. The effect of position and percentage of covering area of mass absorption was studied by the same team of researchers, and their findings were published in the literature [9]. The stiffness effect of the mass layer was investigated by Wang [10]. Furthermore, Liu et al. [11] studied the thickness-shear vibration of a rotated Y-cut quartz crystal plate, in which one of the surfaces was in contact with a viscous fluid layer of finite thickness. The effect of different polarizations of the crystal plate was investigated by Du et al. [12]. However, the research works described above pertained to the uniform mass layer.

Sauerbery's equation gives the linear relationship between the resonance frequency shift of QCM and mass attached on the electrode surface [3]. However, this equation and its various refinements generally assume that

P. Li · F. Jin (✉)
State Key Laboratory for Mechanical Structure Strength and Vibration, School of Aerospace,
Xi'an Jiaotong University, Xi'an 710049, People's Republic of China
E-mail: jinfengzhao@263.net
Fax: +86-29-83237910

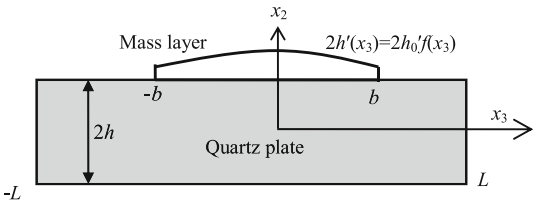

Fig. 1 An AT-cut quartz plate with a partial non-uniform mass layer

the mass is uniform and fully attached to the QCM surfaces [3,9], and it is not a good approximation in practical application. It has been noted that Sauerbery's equation can yield incorrect results when the mass and amplitude of vibration distribution are not uniform, and when the mass is not attached rigidly [13]. When the mass layer is non-uniform or partially distributed on the plate surface, the first-order perturbation integral [14,15] and Mindlin's two-dimensional equation [16–18] can be used to obtain the solution for thickness-shear vibration. Another approximate solution can be obtained by dividing the mass layer into many subsidiary thinner layers [19]. Most of the research works reported are with regard to the thickness-shear (TSh) vibration. In reality, however, due to the finite sizes of devices, pure TSh modes cannot exist in finite crystal plates because of edge effects [20,21]. To the best of the authors' knowledge, there is a lack of relative systematic theoretical results for the anti-plane vibration of crystal plate.

In this article, the anti-plane vibration of an AT-cut quartz plate having an additional partial non-uniform mass layer is solved using the Fourier sine and cosine series solution. The results can be reduced when applied to some special cases, such as the uniform or additional fully attached mass layer. After the convergence is examined, some numerical simulations are carried out based on the solution, while including the frequency shift, the mode number, and the energy-trapping phenomenon. The results reported in this article may enable applications of anti-plane vibrations of crystal devices, for example, QCM, resonators, mass sensors and so on.

2 The anti-plane vibration of the quartz plate and the solution

Consider a crystal mass sensor that comprises a quartz plate with an additional partial non-uniform mass layer, which occupies the region of $-b \le x_3 \le b$ on its upper surface as shown in Fig. 1. The plate is unbounded in the x_1 direction, and only a cross-section of the plate is shown. The length of the plate is $2L$ and the thickness is $2h$. A thin layer of additional mass with the thickness $2h_0' f(x_3)$ and the mass density ρ' is deposited on the surface of the plate. For free vibration frequency analysis, the small piezoelectric coupling is usually not taken into consideration and an elastic analysis is sufficient [16–21]. Anti-plane vibrations in the AT-cut quartz plate were reported by Mindlin [7,20] and can be described as

$$u_1 = u(x_2, x_3, t), \ u_2 = u_3 = 0. \tag{1}$$

Therefore, in the linear theory of piezoelectricity, the corresponding stresses are [22]

$$T_{13} = c_{55}u_{1,3} + c_{56}u_{1,2}, T_{12} = c_{56}u_{1,3} + c_{66}u_{1,2}, \tag{2}$$

where $\boldsymbol{c}$ is the elastic stiffness tensor, and a comma followed by subscript i denotes differentiation with respect to x_i. The governing equation of u_1 is obtained by

$$c_{66}u_{1,22} + c_{55}u_{1,33} + 2c_{56}u_{1,23} = \rho\ddot{u}_1, \tag{3}$$

where ρ is the mass density of the crystal plate, and a dot on top of a symbol represents differentiation with regard to time. For AT-cut quartz plates, $c_{55} = 68.81\times10^9\mathrm{N/m}^2$, $c_{56} = 2.53\times10^9\mathrm{N/m}^2$, and $c_{66} = 29.01\times10^9\mathrm{N/m}^2$ [23]. The value of c_{56} is very small compared with c_{55} and c_{66}; therefore, the usual approximation of neglecting the small c_{56} is followed throughout the rest of the equations discussed in this article [21,24]. Therefore, the governing field equation is

$$u_{1,22} + \frac{c_{55}}{c_{66}}u_{1,33} = \frac{\rho}{c_{66}}\ddot{u}_1. \tag{4}$$

The solution of (4) can be obtained by virtue of the trigonometric function expansion technique along the x_3-axis [25]. Hereafter, $\exp(-i\omega t)$ is omitted for brevity.

$$u_1 = A_1^{(0)}\cos(\eta_0 x_2) + A_2^{(0)}\sin(\eta_0 x_2) + \sum_{m=2,4,6,\ldots}^{\infty}\left[A_1^{(m)}\cos(\eta_m x_2) + A_2^{(m)}\sin(\eta_m x_2)\right]\cos(\alpha_m x_3) + \sum_{m=1,3,5,\ldots}^{\infty}\left[A_3^{(m)}\cos(\eta_m x_2) + A_4^{(m)}\sin(\eta_m x_2)\right]\sin(\alpha_m x_3), \tag{5}$$

where $A_1^{(m)}$, $A_2^{(m)}$, $A_3^{(m)}$ and $A_4^{(m)}$ are undetermined constants, and $\alpha_m = \frac{m\pi}{2L}$, $(m = 0, 1, 2, 3, \ldots)$, and $T_{13} = 0$ at $x_3 = \pm L$ has been satisfied. In this equation, both the cosine series solution and the sine one are all considered. Theoretically, the variation of the thickness of the mass layer can be arbitrary along the x_3-axis in the following discussion [25,26]. Equation (5) satisfies (4) when

$$\eta_m^2 = \frac{\pi^2}{4h^2}\left[\frac{\omega^2}{\omega_s^2} - \frac{c_{55}}{c_{66}}\left(\frac{mh}{L}\right)^2\right], \tag{6}$$

where the resonant frequency of the fundamental mode in an unbounded quartz plate is given by $\omega_s = \frac{\pi}{2h}\sqrt{c_{66}/\rho}$ [23,24]. The shear stress component, which will be used in subsequent boundary conditions, is given as

$$\begin{aligned} T_{12} = {} & c_{66}\eta_0\left[-A_1^{(0)}\sin(\eta_0 x_2) + A_2^{(0)}\cos(\eta_0 x_2)\right] \\ & + c_{66}\sum_{m=2,4,6,\ldots}^{\infty}\eta_m\left[-A_1^{(m)}\sin(\eta_m x_2) + A_2^{(m)}\cos(\eta_m x_2)\right]\cos(\alpha_m x_3) \\ & + c_{66}\sum_{m=1,3,5,\ldots}^{\infty}\eta_m\left[-A_3^{(m)}\sin(\eta_m x_2) + A_4^{(m)}\cos(\eta_m x_2)\right]\sin(\alpha_m x_3). \end{aligned} \tag{7}$$

The boundary conditions at the top and bottom surfaces of the plate are defined by [14,15,19,27]

$$\begin{aligned} & x_2 = h: \quad T_{12} = \begin{cases} -\rho' \cdot 2h_0' f(x_3)\ddot{u}_1, & -b \le x_3 \le b \\ 0, & -L \le x_3 \le -b,\ b \le x_3 \le L \end{cases} \\ & x_2 = -h: \quad T_{12} = 0, \end{aligned} \tag{8}$$

where the mass layer is assumed to be very thin; therefore, only its inertial effect needs to be considered and its stiffness effect can be neglected [27], especially for long waves [10,16–18]. In addition, the mass layer and the quartz plate are perfectly bonded. Substitution of Eqs. (5) and (7) into the boundary conditions (8) yields the following linear homogeneous equations:

$$\begin{aligned} & c_{66}\eta_0\left[-A_1^{(0)}\sin(\eta_0 h) + A_2^{(0)}\cos(\eta_0 h)\right] + c_{66}\sum_{m=2,4,6,\ldots}^{\infty}\eta_m\left[-A_1^{(m)}\sin(\eta_m h) + A_2^{(m)}\cos(\eta_m h)\right]\cos(\alpha_m x_3) \\ & + c_{66}\sum_{m=1,3,5,\ldots}^{\infty}\eta_m\left[-A_3^{(m)}\sin(\eta_m h) + A_4^{(m)}\cos(\eta_m h)\right]\sin(\alpha_m x_3) \\ & = \begin{cases} \rho' 2h_0' f(x_3)\omega^2\left\{\left[A_1^{(0)}\cos(\eta_0 h) + A_2^{(0)}\sin(\eta_0 h)\right]\right. \\ \quad + \sum_{m=2,4,6,\ldots}^{\infty}\left[A_1^{(m)}\cos(\eta_m h) + A_2^{(m)}\sin(\eta_m h)\right]\cos(\alpha_m x_3) \\ \quad \left. + \sum_{m=1,3,5,\ldots}^{\infty}\left[A_3^{(m)}\cos(\eta_m h) + A_4^{(m)}\sin(\eta_m h)\right]\sin(\alpha_m x_3)\right\}, & -b \le x_3 \le b \\ 0, & -L \le x_3 \le -b,\ b \le x_3 \le L \end{cases} \end{aligned} \tag{9}$$

Table 1 The value of ω/ω_s with truncation of the series

n	14	16	18	20	22
$b = 7.5\,\text{mm}$	0.9740933	0.9740925	0.9740909	0.9740899	0.9740899
$R_0 = 3\,\%$	0.9831757	0.9831559	0.9831453	0.9831295	0.9831295
$f(x_3) = 1$	0.9961527	0.9961511	0.9961339	0.9961267	0.9961267
	0.9729317	0.9729313	0.9729301	0.9729301	0.9729301
$b = 10\,\text{mm}$	0.9787835	0.9787579	0.9787559	0.9787489	0.9787481
$R_0 = 3\,\%$	0.9879647	0.9879625	0.9985611	0.9879487	0.9879483
$f(x_3) = 1$	0.9986387	0.9985777	0.9879491	0.9985461	0.9985451
$b = 7.5\,\text{mm}$					
$R_0 = 2\,\%$	0.9832973	0.9832969	0.9832957	0.9832951	0.9832951
$f(x_3) = 1$	0.9913791	0.9913715	0.9913639	0.9913553	0.9913553
	0.9513207	0.9513203	0.9513203	0.9513201	0.9513201
$b = 7.5\,\text{mm}$	0.9668061	0.9667977	0.9667975	0.9667925	0.9667921
$R_0 = 3\%$	0.9839409	0.9839305	0.9839257	0.9839193	0.9839193
$f(x_3) = 2 - \left(\frac{x_3}{b}\right)^2$	0.9998227	0.9996627	0.9996597	0.9996397	0.9996395

$$\eta_0\left[A_1^{(0)}\sin(\eta_0 h) + A_2^{(0)}\cos(\eta_0 h)\right] + \sum_{m=2,4,6,\ldots}^{\infty}\eta_m\left[A_1^{(m)}\sin(\eta_m h) + A_2^{(m)}\cos(\eta_m h)\right]\cos(\alpha_m x_3)$$
$$+ \sum_{m=1,3,5,\ldots}^{\infty}\eta_m\left[A_3^{(m)}\sin(\eta_m h) + A_4^{(m)}\cos(\eta_m h)\right]\sin(\alpha_m x_3) = 0. \tag{10}$$

Multiplying Eqs. (9) and (10) by $\cos(\alpha_n x_3)$ for $n = 0, 2, 4, \ldots$ (with $\alpha_0 = 0$), and $\sin(\alpha_n x_3)$ for $n = 1, 3, 5, \ldots$, respectively, and integrating the resulting equations from $-L$ to L, we obtain the following linear equations for the undetermined constants:

$$\begin{aligned}
&A_1^{(0)}\sin(\eta_0 h) + A_2^{(0)}\cos(\eta_0 h) = 0,\\
&c_{66}\eta_0\left[-A_1^{(0)}\sin(\eta_0 h) + A_2^{(0)}\cos(\eta_0 h)\right]\cdot 2L = \rho' 2h_0\omega^2\left\{\left[A_1^{(0)}\cos(\eta_0 h) + A_2^{(0)}\sin(\eta_0 h)\right]\cdot F_0\right.\\
&\left.+\sum_{m=2,4,6,\ldots}^{\infty}\left[A_1^{(m)}\cos(\eta_m h) + A_2^{(m)}\sin(\eta_m h)\right]\cdot G_m + \sum_{m=1,3,5,\ldots}^{\infty}\left[A_3^{(m)}\cos(\eta_m h) + A_4^{(m)}\sin(\eta_m h)\right]\cdot H_m\right\},\\
&A_1^{(n)}\sin(\eta_n h) + A_2^{(n)}\cos(\eta_n h) = 0,\\
&c_{66}\eta_n\left[-A_1^{(n)}\sin(\eta_n h) + A_2^{(n)}\cos(\eta_n h)\right]\cdot L = \rho' 2h_0\omega^2\left\{\left[A_1^{(0)}\cos(\eta_0 h) + A_2^{(0)}\sin(\eta_0 h)\right]\cdot G_n\right.\\
&\left.+\sum_{m=2,4,6,\ldots}^{\infty}\left[A_1^{(m)}\cos(\eta_m h)+A_2^{(m)}\sin(\eta_m h)\right]\cdot S_{mn}+\sum_{m=1,3,5,\ldots}^{\infty}\left[A_3^{(m)}\cos(\eta_m h)+A_4^{(m)}\sin(\eta_m h)\right]\cdot T_{mn}\right\},\\
&A_3^{(n)}\sin(\eta_n h) + A_4^{(n)}\cos(\eta_n h) = 0,\\
&c_{66}\eta_n\left[-A_3^{(n)}\sin(\eta_n h) + A_4^{(n)}\cos(\eta_n h)\right]\cdot L = \rho' 2h_0\omega^2\left\{\left[A_1^{(0)}\cos(\eta_0 h) + A_2^{(0)}\sin(\eta_0 h)\right]\cdot H_n\right.\\
&\left.+\sum_{m=2,4,6,\ldots}^{\infty}\left[A_1^{(m)}\cos(\eta_m h)+A_2^{(m)}\sin(\eta_m h)\right]\cdot T_{mn}+\sum_{m=1,3,5,\ldots}^{\infty}\left[A_3^{(m)}\cos(\eta_m h)+A_4^{(m)}\sin(\eta_m h)\right]\cdot Q_{mn}\right\},
\end{aligned} \tag{11}$$

where

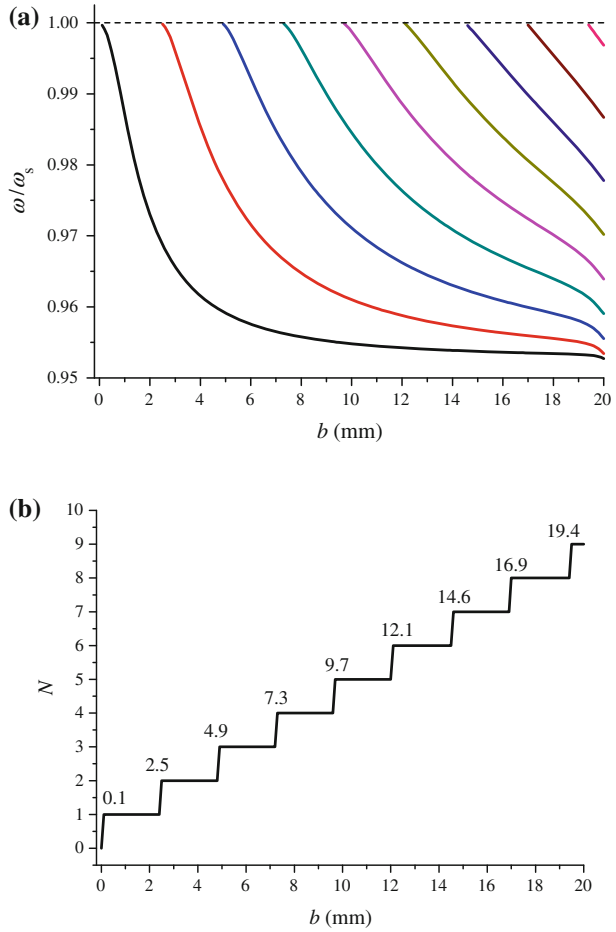

Fig. 2 The frequency ratio ω/ω_s and the mode number N of the anti-plane vibration of quartz plate when the length of the mass layer changes ($R_0 = 5\,\%$, $f(x_3) = 1$). **a** The frequency ratio ω/ω_s; **b** The mode number N

$$
\begin{aligned}
F_0 &= \int_{-b}^{b} f(x_3)\mathrm{d}x_3, \\
G_m &= \int_{-b}^{b} f(x_3)\cos(\alpha_m x_3)\mathrm{d}x_3\ ,\ \ (m = 2, 4, 6, \ldots), \\
H_m &= \int_{-b}^{b} f(x_3)\sin(\alpha_m x_3)\mathrm{d}x_3\ ,\ \ (m = 1, 3, 5, \ldots), \\
S_{mn} &= \int_{-b}^{b} f(x_3)\cos(\alpha_m x_3)\cos(\alpha_n x_3)\mathrm{d}x_3\ ,\ \ (m = 2, 4, 6, \ldots,\ n = 2, 4, 6, \ldots), \\
T_{mn} &= \int_{-b}^{b} f(x_3)\sin(\alpha_m x_3)\cos(\alpha_n x_3)\mathrm{d}x_3\ ,\ \ (m = 1, 3, 5, \ldots,\ n = 2, 4, 6, \ldots), \\
Q_{mn} &= \int_{-b}^{b} f(x_3)\sin(\alpha_m x_3)\sin(\alpha_n x_3)\mathrm{d}x_3\ ,\ \ (m = 1, 3, 5, \ldots,\ n = 1, 3, 5, \ldots).
\end{aligned}
\tag{12}
$$

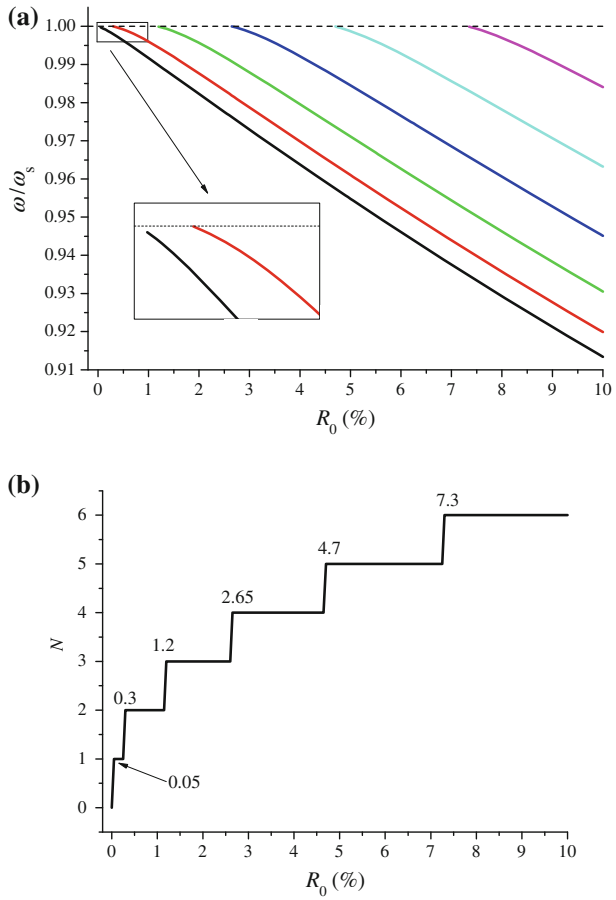

Fig. 3 The frequency ratio ω/ω_s and the mode number N of the anti-plane vibration of quartz plate when the mass fraction of the layer changes ($b = 10.0\,\text{mm}$, $f(x_3) = 1$). **a** The frequency ratio ω/ω_s; **b** The mode number N

Eliminating $A_2^{(0)}$, $A_2^{(m)}$, and $A_4^{(m)}$ from Eq. (11) and introducing the factor $R_0 = \frac{2\rho' h_0'}{2\rho h}$, the following equations can be obtained with regard to $A_1^{(0)}$, $A_1^{(m)}$, and $A_3^{(m)}$:

$$\left[\frac{\omega^2}{\omega_s^2}\beta_0 \cot(2\eta_0 h)\frac{F_0}{2L}+1\right]A_1^{(0)}+\sum_{m=2,4,6,\ldots}^{\infty}\left(\frac{\omega^2}{\omega_s^2}\beta_0\gamma_{(m,0)}\frac{G_m}{2L}\right)A_1^{(m)}+\sum_{m=1,3,5,\ldots}^{\infty}\left(\frac{\omega^2}{\omega_s^2}\beta_0\gamma_{(m,0)}\frac{H_m}{2L}\right)A_3^{(m)}=0$$

$$\frac{\omega^2}{\omega_s^2}\beta_n\gamma_{(0,n)}\frac{G_n}{L}A_1^{(0)}+\sum_{m=2,4,6,\ldots}^{\infty}\left(\frac{\omega^2}{\omega_s^2}\beta_n\gamma_{(m,n)}\frac{S_{mn}}{L}+\delta_{mn}\right)A_1^{(m)}+\sum_{m=1,3,5,\ldots}^{\infty}\left(\frac{\omega^2}{\omega_s^2}\beta_n\gamma_{(m,n)}\frac{T_{mn}}{L}\right)A_3^{(m)}=0,$$

$$(n = 2, 4, 6, \ldots) \tag{13}$$

$$\frac{\omega^2}{\omega_s^2}\beta_n\gamma_{(0,n)}\frac{H_n}{L}A_1^{(0)}+\sum_{m=2,4,6,\ldots}^{\infty}\left(\frac{\omega^2}{\omega_s^2}\beta_n\gamma_{(m,n)}\frac{T_{mn}}{L}\right)A_1^{(m)}+\sum_{m=1,3,5,\ldots}^{\infty}\left(\frac{\omega^2}{\omega_s^2}\beta_n\gamma_{(m,n)}\frac{Q_{mn}}{L}+\delta_{mn}\right)A_3^{(m)}=0,$$

$$(n = 1, 3, 5, \ldots)$$

in which $\beta_n = \frac{\pi^2 R_0}{2h\eta_n}$, and $\gamma_{(m,n)} = \frac{\cos(2\eta_m h)}{2\cos(\eta_m h)\sin(\eta_n h)}$ with $m = 0, 1, 2, 3, \ldots,\ n = 0, 1, 2, 3, \ldots$. For non-trivial solutions, the determinant of the coefficient matrix has to vanish, and from this the frequency can be obtained.

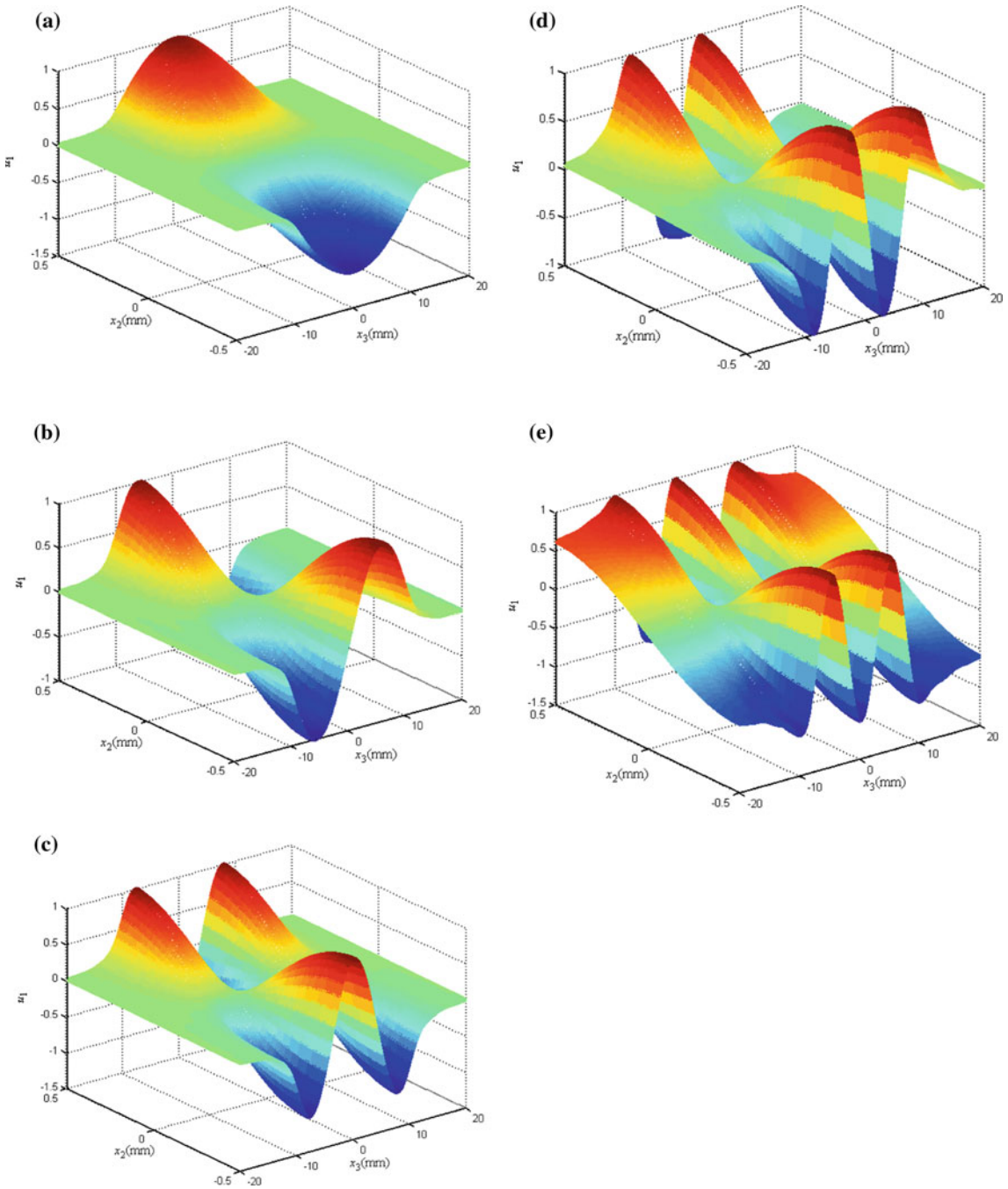

Fig. 4 The relative displacement u_1 of the first five modes of the quartz plate ($b = 10.0\,\text{mm}$, $R_0 = 5\,\%$, $f(x_3) = 1$). **a** 1st mode, $\omega = 0.9548103\omega_s$; **b** 2nd mode, $\omega = 0.9610253\omega_s$; **c** 3rd mode, $\omega = 0.9711165\omega_s$; **d** 4th mode, $\omega = 0.9845225\omega_s$; **e** 5th mode, $\omega = 0.9987597\omega_s$

If the partial non-uniform mass layer is symmetric about x_2-axis, then $H_m = T_{mn} = 0$ can be obtained from Eq. (12). Equation (13) can be reduced as

$$\begin{aligned}\left[\frac{\omega^2}{\omega_s^2}\beta_0\cot(2\eta_0 h)\frac{F_0}{2L}+1\right]A_1^{(0)}+\sum_{m=1,2,3,\ldots}^{\infty}\left(\frac{\omega^2}{\omega_s^2}\beta_0\gamma_{(m,0)}\frac{G_m}{2L}\right)A_1^{(m)} &= 0,\\ \frac{\omega^2}{\omega_s^2}\beta_n\gamma_{(0,n)}\frac{G_n}{L}A_1^{(0)}+\sum_{m=1,2,3,\ldots}^{\infty}\left(\frac{\omega^2}{\omega_s^2}\beta_n\gamma_{(m,n)}\frac{S_{mn}}{L}+\delta_{mn}\right)A_1^{(m)} &= 0,\end{aligned} \tag{14a}$$

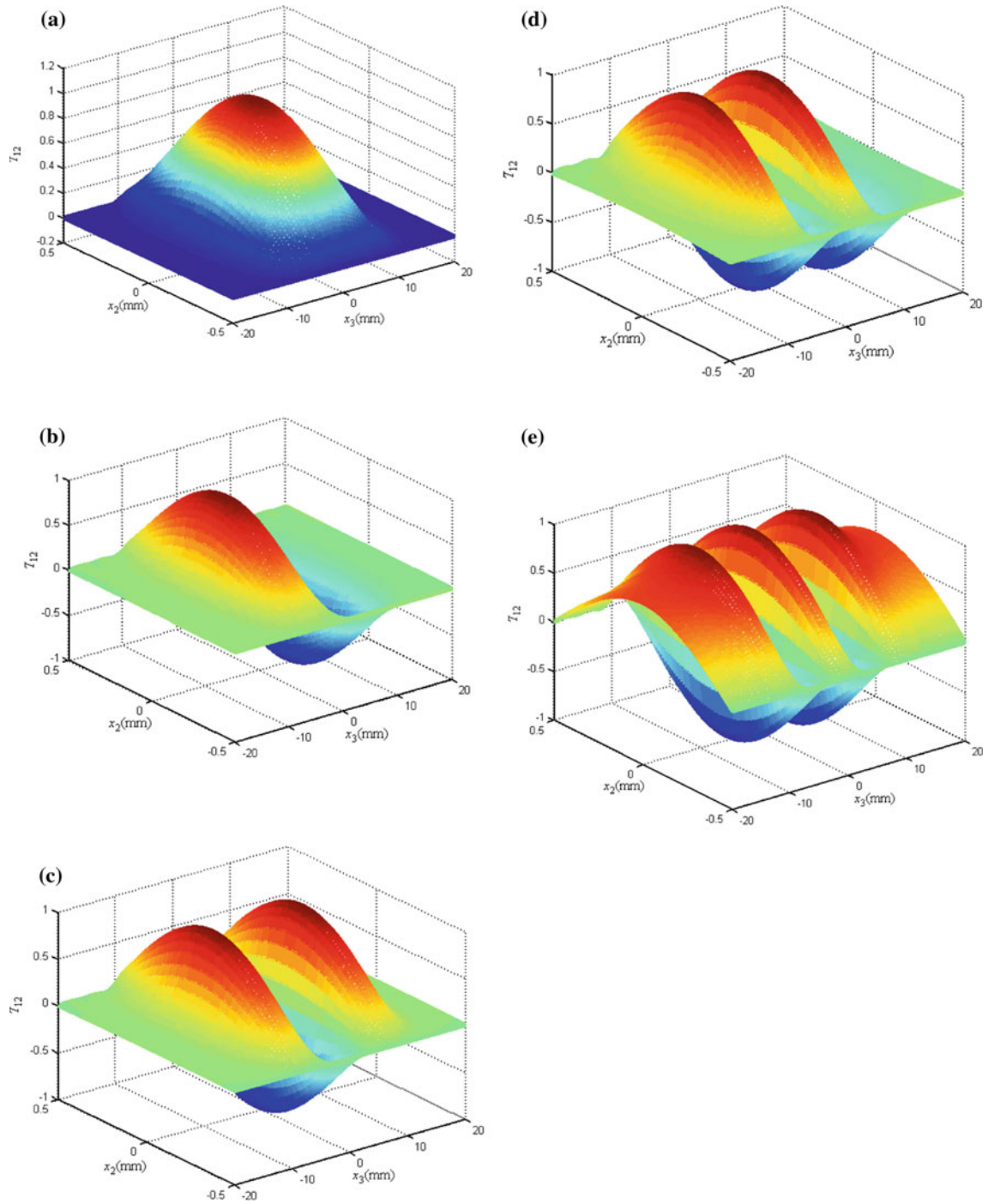

Fig. 5 The relative stress component T_{12} of the first five modes of the quartz plate ($b = 10.0\,\text{mm}$, $R_0 = 5\,\%$, $f(x_3) = 1$). **a** 1st mode, $\omega = 0.9548103\omega_s$; **b** 2nd mode, $\omega = 0.9610253\omega_s$; **c** 3rd mode, $\omega = 0.9711165\omega_s$; **d** 4th mode, $\omega = 0.9845225\omega_s$; **e** 5th mode, $\omega = 0.9987597\omega_s$

with $\alpha_m = \frac{m\pi}{L}$, $(m = 0, 1, 2, 3, \ldots)$, or

$$\sum_{m=1,3,5,\ldots}^{\infty} \left(\frac{\omega^2}{\omega_s^2} \beta_n \gamma_{(m,n)} \frac{Q_{mn}}{L} + \delta_{mn} \right) A_3^{(m)} = 0 \tag{14b}$$

for $n = 1, 3, 5, \ldots$.

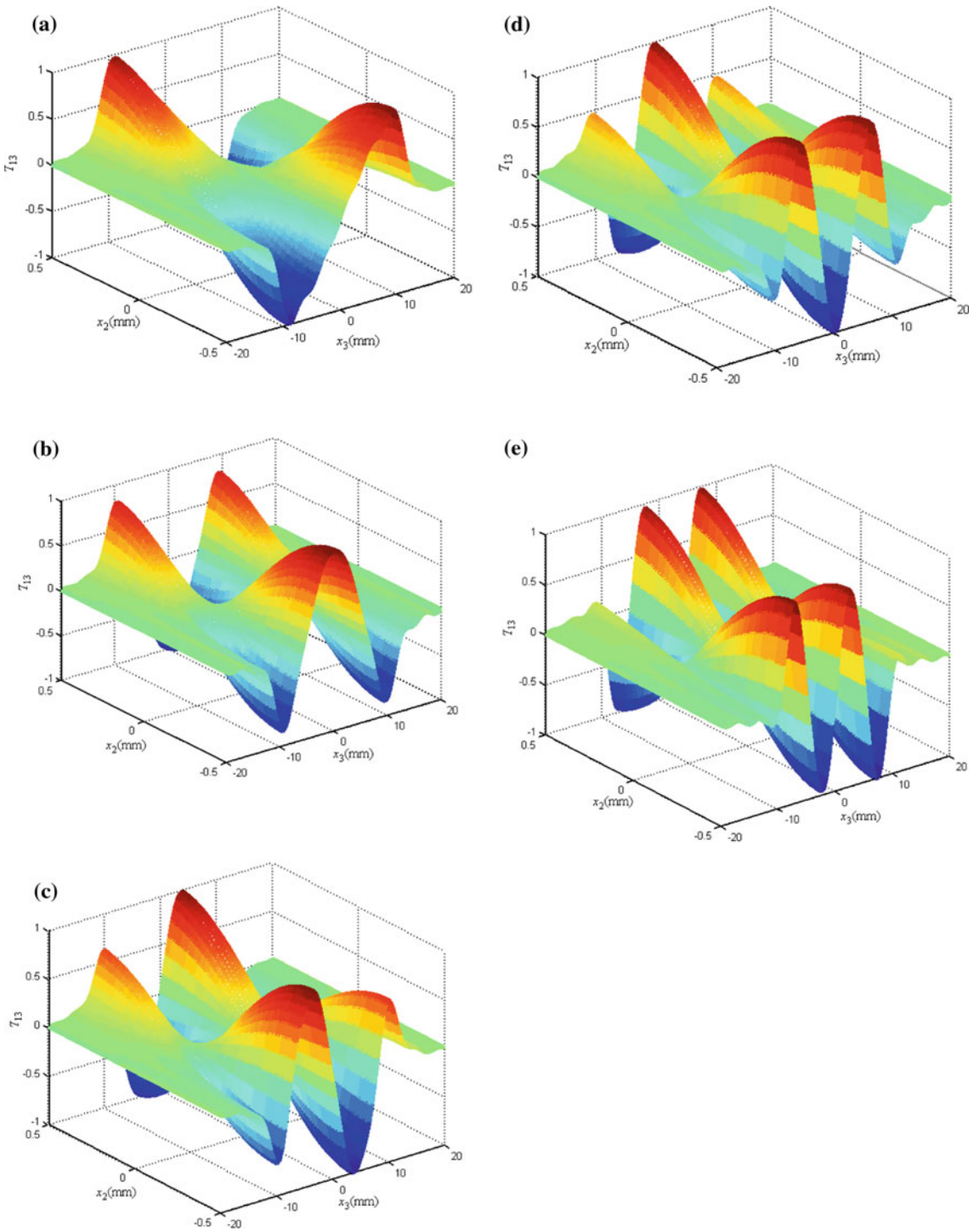

Fig. 6 The relative stress component T_{13} of the first five modes of the quartz plate ($b = 10.0\,\text{mm}$, $R_0 = 5\,\%$, $f(x_3) = 1$). **a** 1st mode, $\omega = 0.9548103\omega_s$; **b** 2nd mode, $\omega = 0.9610253\omega_s$; **c** 3rd mode, $\omega = 0.9711165\omega_s$; **d** 4th mode, $\omega = 0.9845225\omega_s$; **e** 5th mode, $\omega = 0.9987597\omega_s$

Equation (14a) determines the frequencies of the symmetric waves, and Eq. (14b) is used to solve the anti-symmetric waves. Furthermore, if the mass layer is uniform, $F_0 = 2b$ and $G_m = \frac{2L}{m\pi}\sin(\frac{m\pi a}{L})$ can be obtained from Eq. (12). Hence, Eq. (14a) is the same as those described in the work by Kong et al. [24]. As a special case, if the homogeneous mass layer encompasses the whole surface of the quartz plate, that is, $b = L$, then $F_0 = 2L$, $G_m = 0$, and $S_{mn} = L\delta_{mn}$. Thus, Eq. (14a) can be abbreviated as

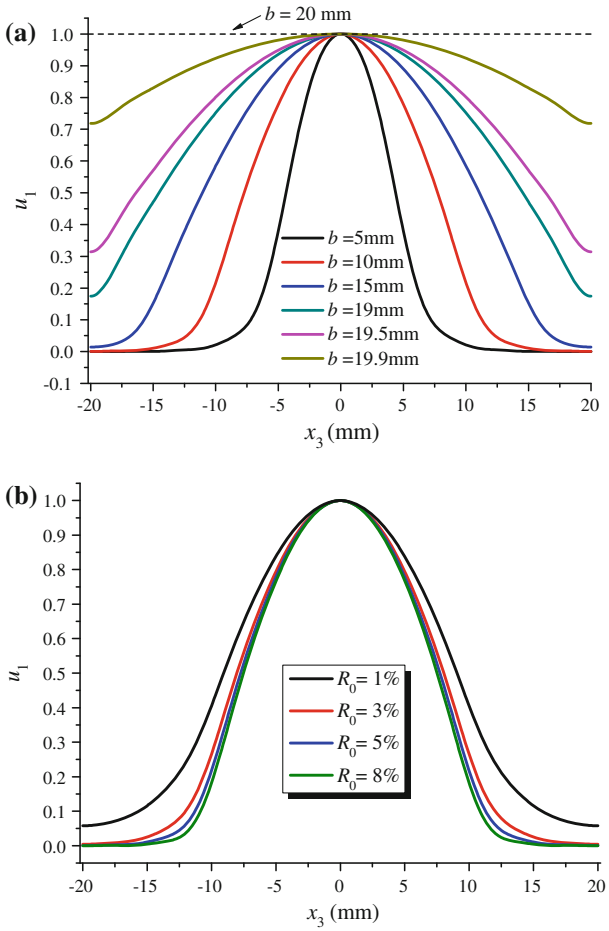

Fig. 7 The relative displacement u_1 of the first mode along x_3 direction when $x_2 = h$ and $f(x_3) = 1$. **a** for some selected b ($R_0 = 5\,\%$); **b** for some selected R_0 ($b = 10.0\,\text{mm}$)

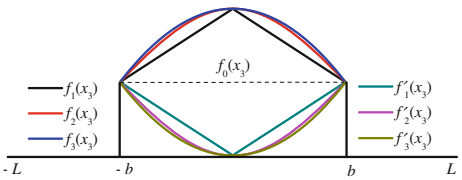

Fig. 8 The shapes of the non-uniform mass layer ($b = 10.0\,\text{mm}$, $R_0 = 5\,\%$)

$$\frac{\omega^2}{\omega_s^2} \cdot \beta_0 + \tan(2\eta_0 h) = 0, \tag{15}$$

which is the same as the outcome discussed by Chen et al. [28].

3 Numerical simulation

For a numerical example, an AT-cut quartz plate with the half length $L = 20\,\text{mm}$, the thickness $2h = 1\,\text{mm}$ and the mass density of $\rho = 2{,}649\,\text{kg/m}^3$ is considered. Generally speaking, Eq. (13) is a transcendental equation, in which the frequency cannot be solved using an explicit expression. Hence, we have adopted the following iterative procedure for numerical computations [29]. For an initial value of ω, we evaluate the determinant of the coefficient matrix, presented in the left hand of Eq. (13), for various values of the unknown quantity,

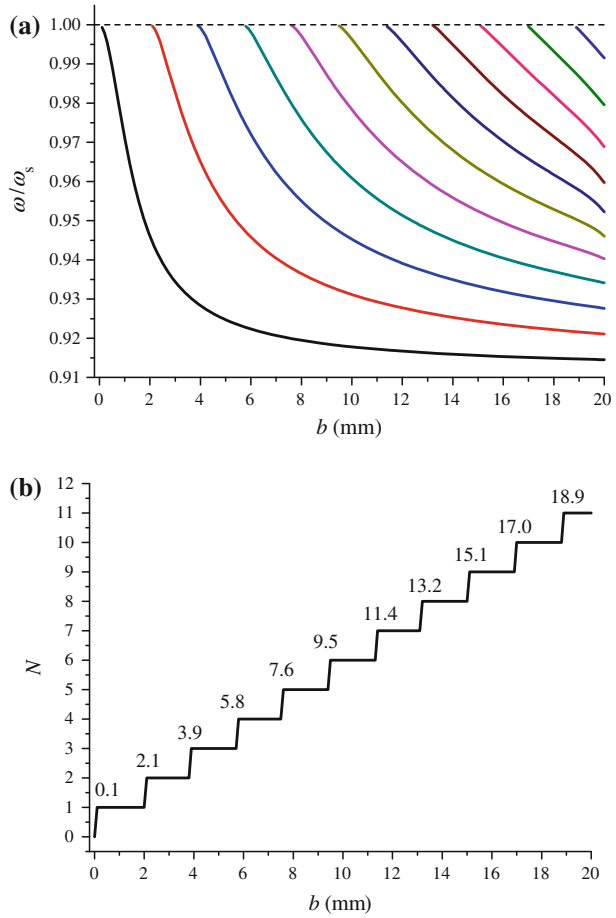

Fig. 9 The frequency ratio ω/ω_s and the mode number N of the anti-plane vibration of quartz plate when the length of the mass layer changes ($R_0 = 5\,\%$, $f_3(x_3) = 2 - (\frac{x_3}{b})^2$). **a** The frequency ratio ω/ω_s; **b** The mode number N

and each time adding a fixed but small increment to that unknown quantity till the value of the determinant changes its sign. Then, the "bisection method" is applied to locate the root correct to a chosen number of decimal places.

In the following discussion, we mainly focus on energy-trapping phenomenon, that is, $\omega_s(1-R_0) < \omega < \omega_s$ for the uniform mass layer [24]. However, if the thickness is variable, the relation $\omega_s(1-\mu R_0) < \omega < \omega_s$ is used for the seeking of the frequency, in which μ is selected for different variation form of mass layer.

3.1 Convergence and verification of the series

First of all, we examined the convergence and verification of the series. In practical applications, R_0 is usually less than 1 % [23]. An exaggerated value of R is selected to show its numerical effects more clearly [21,23,28]. Table 1 shows the frequencies of the mass sensor for some special cases by using the trigonometric function expansion method. In such cases, the corresponding frequencies converge very well, which can be seen from this table. On the other hand, the parameter b, R_0, and surface shape of the mass layer hardly affect the convergence of the series. Therefore, all calculations below are based on calculations using 22 terms in the series. Meanwhile, $\eta_m^2 (m = 0, 1, 2, 3, \ldots)$ is positive in this case, which reduces the complexity of numerical simulation. When a large m is indeed needed, η_m^2 can be redefined with a minus sign and the sine and cosine functions in Eq. (5) can be changed to hyperbolic sine and cosine functions, respectively [21].

Taking the case of $b = 7.5\,\text{mm}$, $R_0 = 3\,\%$, $f(x_3) = 1$ for example, three resonant frequencies $\omega_1/\omega_s = 0.974090$, $\omega_2/\omega_s = 0.983130$, and $\omega_3/\omega_s = 0.996127$ are found within $\omega_s(1 - R_0) < \omega < \omega_s$. The frequen-

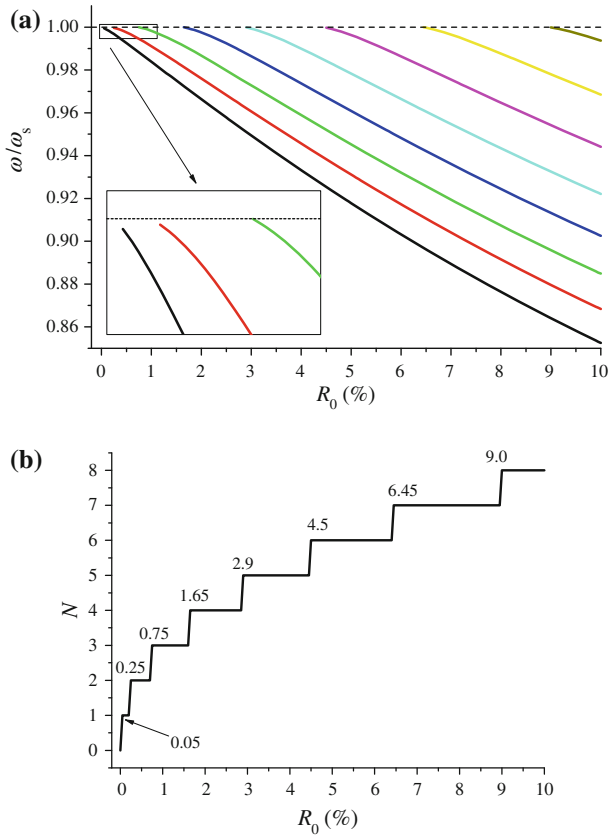

Fig. 10 The frequency ratio ω/ω_s and the mode number N of the anti-plane vibration of quartz plate when the mass fraction of the layer changes ($b = 10.0\,\text{mm}$, $f_3(x_3) = 2 - (\frac{x_3}{b})^2$). **a** The frequency ratio ω/ω_s; **b** The mode number N

cies of two symmetric modes ω_1 and ω_3 are nearly the same as those discussed by Kong et al. [24], and this validates the accuracy of our calculation to some extent.

3.2 The uniform mass layer

In this section, we consider the uniform mass layer, that is, $f_0(x_3) = 1$. Figures 2a and 3a show the variation pattern of non-dimensional frequency ratio ω/ω_s with the parameter b and R_0, respectively. At this time, Figs. 2b and 3b give the mode number curves under the same conditions, in which the quantitative values appeared in these figures are corresponding values when the new modes appear. All these frequencies of the anti-plane vibration initiate the unbounded quartz plate ω_s and approach the value $\omega_s(1 - R_0)$ with the increasing b and R_0, which means the longer or thicker mass layer decreases the limit value of the frequency and makes more modes trapped in this region. However, the minimum cannot reach $\omega_s(1 - R_0)$, which is because the value is the resonant frequency of the fundamental TSh mode in an unbounded quartz plate fully covered by a uniform mass layer at the plate top surface [23,24]. Here, the size of the plate in the x_3 direction is a finite dimension, not unbounded. In general, the frequency changes nonlinearly with b, but it is quasi-linear especially for the larger R_0. When R_0 is small, this kind of nonlinearity takes notable. On the other hand, higher modes appear periodically with the increasing of b, which can be seen from Fig. 2b. For instance, the second mode appears at $b = 2.5\,\text{mm}$; the third one emerges at $b = 4.9\,\text{mm}$; the forth one takes at $b = 7.3\,\text{mm}$, etc. The period of Δb is about 2.4 mm. However, this kind of periodical character does not happen with the increasing of R_0 in Fig. 3b.

Here, we choose $b = 10\,\text{mm}$ and $R_0 = 5\,\%$ for an instance. b is related to the length of mass layer, and R_0 is corresponding to the product of mass density and thickness. There exist five trapped modes for the partial uniform mass layer: $\omega_1 = 0.9548103\omega_s$, $\omega_2 = 0.9610253\omega_s$, $\omega_3 = 0.9711165\omega_s$, $\omega_4 = 0.9845225\omega_s$, and $\omega_5 = 0.9987597\omega_s$. Figures 4, 5, and 6 show the relative displacement component u_1, stress components T_{12} and T_{13} of these modes. The values of the displacement and stress components are normalized in such a way

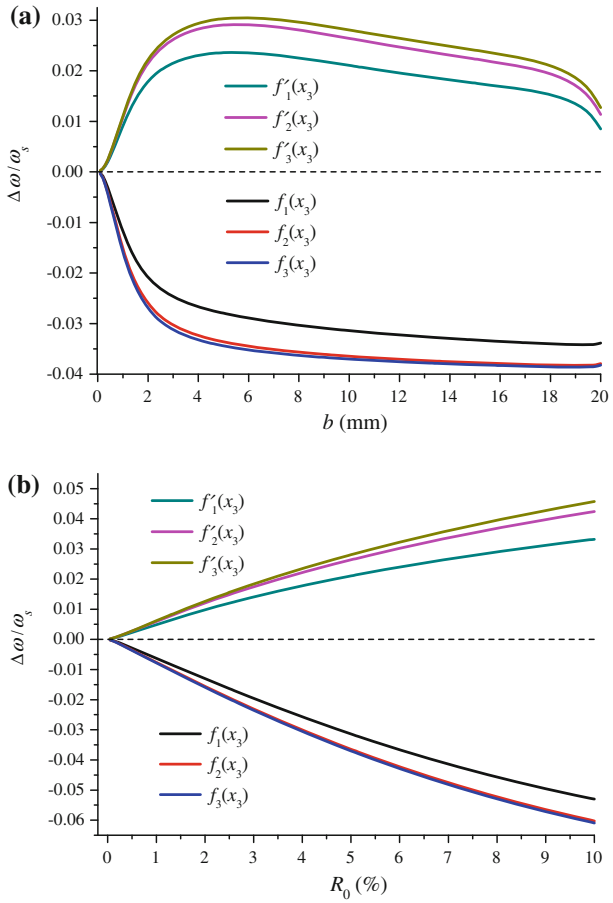

Fig. 11 The non-dimensional frequency shift $\Delta\omega/\omega_s$ of the first mode due to the surface shape of mass layer. **a** with b ($R_0 = 5\,\%$); **b** with R_0 ($b = 10.0\,\text{mm}$)

that the maximal displacement is equal to one [16,19,21]. Hence, the relative displacement component u_1, stress components T_{12} and T_{13} in this text are all non-dimensional numbers physically. The odds modes are symmetric about the x_2-axis, and the even modes are anti-symmetric waves for u_1 and T_{12}. For T_{13}, it is just opposite. In the region of $|x_3| > b$, u_1 and T_{13} are almost equal to zero, which is related to the energy-trapping phenomenon. The vibration is confined to the central portion of the plate, that is, the region with the mass layer, and essentially, there is almost no vibration in the rest of the plate. Meanwhile, T_{12} is also trapped in the x_2 direction, which can be seen from Fig. 5.

Figure 7 shows the effects of the parameters b and R_0 on the relative displacement component u_1 of the fundamental mode, that is, the first mode in this text, which is the usual operating mode of a resonator. The length of the mass layer determines the region of energy distribution. Shorter mass layer makes energy trapped in the center of the plate easily, which can be seen from Fig. 7a. Meanwhile, a larger thicker mass layer, that is, bigger R_0, makes more energy concentrate in the center region. In other words, the effect of b on the energy trapping is more evident than that of R_0 for the uniform mass layer. To the point, if the mass layer is too long, for example, $b = 19\,\text{mm}$, the vibration will not approach to zero even at the edge of the plate. Especially, when the quartz plate is fully covered by a uniform mass layer, that is, $b = L = 20\,\text{mm}$, the amplitude of vibration keeps constant along the x_3-direction at the surface of the plate, which means the energy-trapping phenomenon completely disappears.

3.3 The effect of inhomogeneous mass layer

With the exception of the uniform thickness, the effect of the thickness on the frequencies and displacement components when the non-uniform mass layer changes in terms of linear, cosine, and quadratic functions is considered separately. For the uniform mass layer,

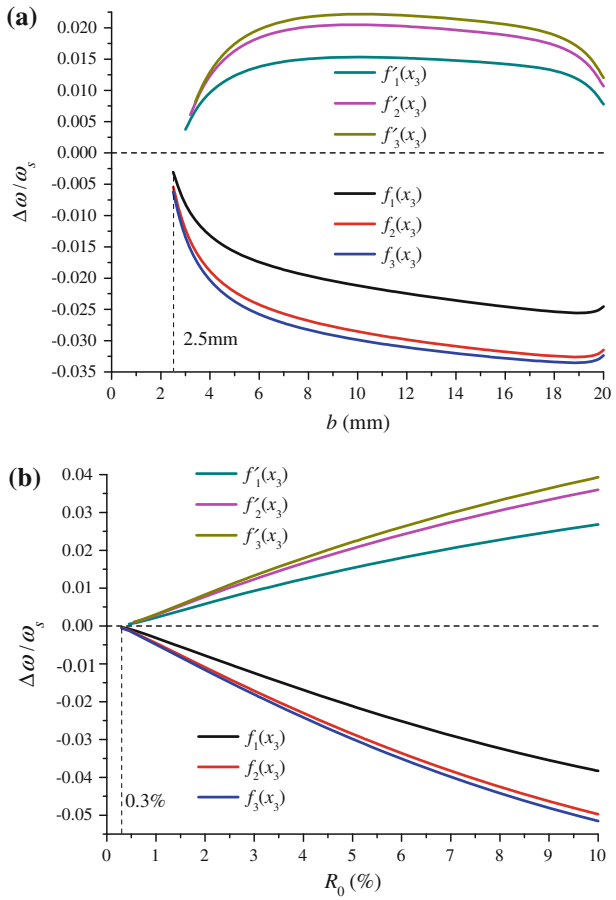

Fig. 12 The non-dimensional frequency shift $\Delta\omega/\omega_s$ of the second mode due to the surface shape of mass layer. **a** with $b(R_0 = 5\,\%)$; **b** with R_0 ($b = 10.0\,\text{mm}$)

$$f_0(x_3) = 1. \tag{16}$$

Meanwhile, if the mass layer is thicker at the center than the edge,

$$f_1(x_3) = \begin{cases} 2 + x_3/b, & -b < x_3 < 0, \\ 2 - x_3/b, & 0 < x_3 < b, \end{cases} \tag{17a}$$

$$f_2(x_3) = 1 + \cos\left(\frac{\pi}{2b}x_3\right), \tag{17b}$$

$$f_3(x_3) = 2 - \left(\frac{x_3}{b}\right)^2. \tag{17c}$$

Oppositely, if the mass layer is thinner at the center than the edge,

$$f'_1(x_3) = \begin{cases} -x_3/b, & -b < x_3 < 0, \\ x_3/b, & 0 < x_3 < b, \end{cases} \tag{18a}$$

$$f'_2(x_3) = 1 - \cos\left(\frac{\pi}{2b}x_3\right), \tag{18b}$$

$$f'_3(x_3) = \left(\frac{x_3}{b}\right)^2. \tag{18c}$$

The surface shape of the mass layer is shown in Fig. 8 when $b = 10\,\text{mm}$ and $R_0 = 5\,\%$. In this presentation, $\mu = 2$ is adequate for the three non-uniform layers of Eq. (17), and for Eq. (18), $\mu = 1$ is used to solve the frequency. Figures 9 and 10 give the frequency ratio ω/ω_s and the mode number N of the anti-plane vibration

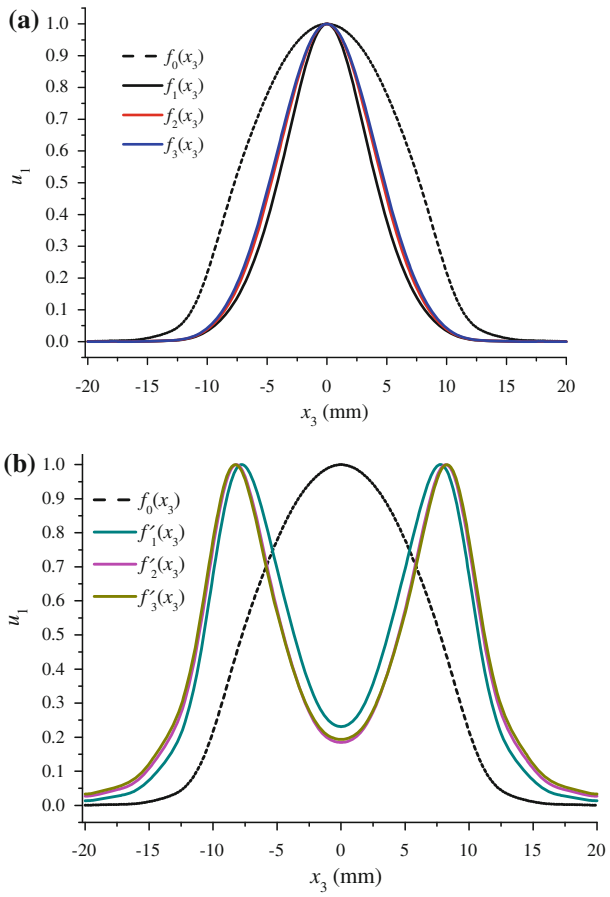

Fig. 13 The comparison of relative displacement u_1 of the first mode along the x_3 direction when $x_2 = h$ ($b = 10\,\text{mm}$, $R_0 = 5\,\%$). **a** for $f_0(x_3)$, $f_1(x_3)$, $f_2(x_3)$ and $f_3(x_3)$; **b** for $f_0(x_3)$, $f'_1(x_3)$, $f'_2(x_3)$ and $f'_3(x_3)$

of the quartz plate with the increasing of b and R_0, respectively, when the mass layer changes in the quadratic function of $f_3(x_3)$. The resonance frequencies have the same variation tendency as the uniform mass layer. The frequencies initiate the unbounded quartz plate ω_s with the increasing b and R_0. However, the lower limit value of frequencies is $\omega_s(1 - \mu R_0)$, where $1 \leq \mu \leq 2$ and is related to the area of the mass layer. Besides, there are eleven modes when b equals to L. The mode number excited in the plate with greater inertia is larger than the uniform circumstance. Higher modes take place periodically with the increasing of b, and the period is $\Delta b = 1.9\,\text{mm}$, which is smaller than the uniform mass layer. If the mass layer is thinner at the center than the edge, that is, $f'_3(x_3)$, the changing variation is opposite. For example, there are only three modes excited when $b = L : \omega_1 = 0.9654415\omega_s$, $\omega_2 = 0.9899405\omega_s$, and $\omega_3 = 0.9900289\omega_s$. The corresponding figures are not listed for the sake of brevity.

The frequency shift due to the additional thickness when compared with the uniform layer can be defined as $\Delta\omega = \omega - \omega_{f_0}$, where ω_{f_0} is the frequency of the plate with the uniform mass layer and $\omega = \omega_{f_i}$ or $\omega = \omega_{f'_i}(i = 1, 2, 3)$ represents the frequency of the plate with the non-uniform mass layer. The non-dimensional frequency $\Delta\omega/\omega_s$ of the first and second modes with b and R_0 is depicted in Figs. 11 and 12, respectively. This is different in our study from the definitions in previously published reports in the literature [3,5,15–19]. There are two reasons. Firstly, ω_s remains constant across these cases, and Figs. 11 and 12 would be identical to Figs. 2 and 3 if the same definition is applied. Secondly, we mainly focus on the frequency shift due to the change of its thickness compared with the uniform mass layer.

From Figs. 11 and 12, it can be concluded that the frequency shifts of the first modes initiate zero for the functions described above. However, the initial value of b and R_0 are no longer null for the second modes (in this case, the same tendency can be seen for the higher modes; therefore, only the second mode is depicted), which is because larger b and R_0 make the higher modes appear earlier, as shown in Figs. 9 and 10.

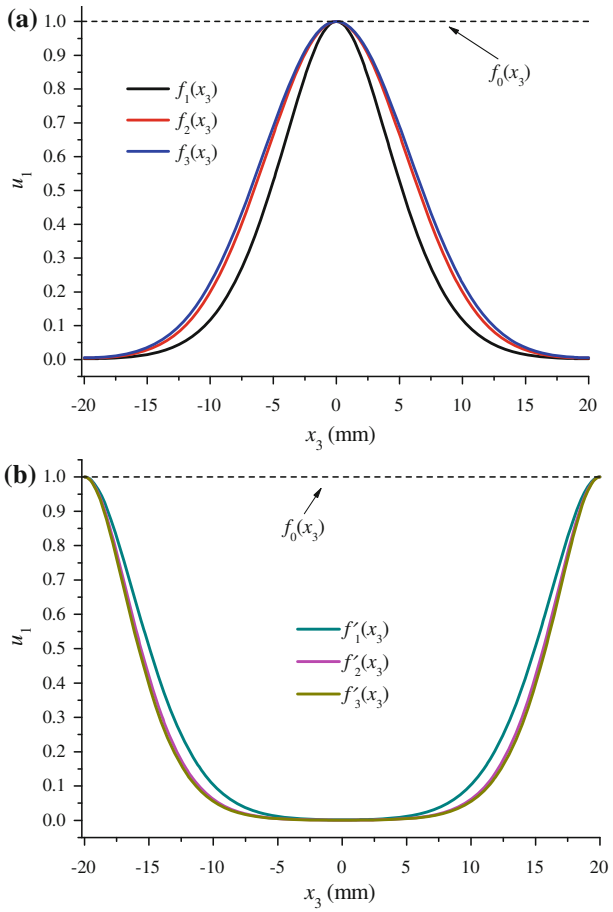

Fig. 14 The comparison of relative displacement u_1 of the first mode along x_3 direction when $x_2 = h(b = 20\,\text{mm}, R_0 = 5\,\%)$. **a** for $f_0(x_3)$, $f_1(x_3)$, $f_2(x_3)$ and $f_3(x_3)$; **b** for $f_0(x_3)$, $f'_1(x_3)$, $f'_2(x_3)$ and $f'_3(x_3)$

On the other hand, compared with the uniform mass layer, a thicker mass layer with greater inertia lowers the resonance frequency and a thinner one increases the frequency. Taking $f_1(x_3)$ and $f'_1(x_3)$ for example, the surface shapes are symmetric about $f_0(x_3)$, but the frequency shift is not symmetric. Particularly for the different lengths of the mass layer, the frequency shifts are non-monotonous. They decrease or increase first and then turn to ascend or descend curves when the mass layer nearly covers the whole quartz plate. However, for different R_0, the frequency shifts are quasi-linear. Meanwhile, because the shapes of the layers are nearly the same (Fig. 8), the cosine and quadratic functions have almost the same frequency shifts.

The relative displacement component of the upper surface of the plate along the x_3-axis, when $b = 10.0\,\text{mm}$ and $R_0 = 5\,\%$, is considered for different layers, as shown in Fig. 13. The energy-trapping phenomenon is obvious for the circumstances above and is attributable to the additional partial mass layer. Especially for the thinner mass layer at the center, the displacement of the fundamental mode is symmetric on the x_2-axis, but with two peaks.

Finally, in order to explain the reason that the frequency shifts in Figs. 11 and 12 change evidently when the non-uniform mass layer is nearly fully attached on the surface of the plate, we give the relative displacement of the fundamental mode along the x_3-axis when $b = L$ and $R_0 = 5\,\%$. The vibration of the plate with a uniform mass layer will keep constant under this condition, as Fig. 7a, which means no energy trapping. However, if the center of the mass layer is thicker than the edge, energy-trapping phenomenon appears again because of the change of surface shape of mass layer (Fig. 14a). For the mass layer with thinner thickness at the center than the edge, the vibration reaches maximum at the edge of the plate, and the energy is concentrated at these regions (Fig. 14b).

4 Conclusions

The trigonometric series method, which gives good convergence and high precision, is employed for solving the problem of anti-plane vibration of a quartz plate with several types of additional partial non-uniform mass layers on its surface, with the interface perfectly bonding. The frequency spectrums with the length and mass fraction of mass layer are discussed separately. The energy-trapping phenomenon is displayed although the mass layer is non-homogeneous. All the results obtained may give theoretical guidance not only for physical phenomena explanations but also for experimental measurement of layer properties in mass sensor devices.

In the present contribution, we discussed the anti-plane vibration of a finite quartz plate in the x_3-direction, and hence, the small coupling elastic constant c_{56} is neglected for simplification. Generally speaking, ignoring the small c_{56} may have influence on the values of the frequencies of these trapped modes, but will not affect the physical essence of the anti-plane vibration of a quartz plate with an additional non-uniform mass layer, such as the modes number, frequency tendency, displacement distribution, energy trapping, and so on. Further research concerning the effect of small c_{56} on the above-mentioned phenomenon for sensing applications needs to be carried out in the future.

Acknowledgments The financial support of the work by the National Natural Science Foundation of China (No. 11272247) and the National 111 Project of China (No. B06024), and Scholarship Award for Excellent Doctoral Student granted by Ministry of Education are gratefully acknowledged.

References

1. Kosinski, J.A.: Thickness vibrations of flat piezoelectric plates with massy electrodes of unequal thickness. In: Proceedings of IEEE Ultrasonics Symposium, pp. 70–73 (2003)
2. Miller, J.G., Bolef, D.I.: Acoustic wave analysis of the operation of quartz-crystal film-thickness monitors. J. Appl. Phys. **39**, 5815–5816 (1968)
3. Sauerbrey, G.Z.: Use of quartz vibrator for weighing thin films on a microbalance. Z. Physik **155**, 206–222 (1959)
4. Boersma, F., Van Ballegooyen, E.C.: Rotated Y-cut quartz crystal with two different electrodes treated as a one-dimensional acoustic composite resonator. J. Acoust. Soc. Am. **62**, 335–340 (1977)
5. Yang, J., Yang, Z.: Analytical and numerical modeling of resonant piezoelectric devices in China—a review. Sci. China Ser. G-Phys. Mech. Astron. **51**, 1775–1807 (2008)
6. Vander Steen, C., Boersma, F., Van Ballegooyen, E.C.: The influence of mass loading outside the electrode area on the resonant frequencies of a quartz-crystal microbalance. J. Appl. Phys. **48**, 3201–3205 (1977)
7. Mindlin, R.D., Lee, P.C.Y.: Thickness-shear and flexural vibrations of partially plated, crystal plates. Int. J. Solids Struct. **2**, 125–139 (1966)
8. Lu, P., Shen, F., Chen, H.: A theoretical analysis of mechanical dissipation of an electroded quartz resonator. IEEE Trans. Ultrason. Ferroelectr. Freq. Control **50**, 1069–1072 (2003)
9. Lu, F., Lee, H.P., Lim, S.P.: Quartz crystal microbalance with rigid mass partially attached on electrode surfaces. Sensor. Actuat. A-Phys. **112**, 203–210 (2004)
10. Wang, J.: Consideration of stiffness and mass effects of relatively thicker electrodes with Mindlin plate theory. IEEE Trans. Ultrason. Ferroelectr. Freq. Control **53**, 1218–1221 (2006)
11. Liu, B., Jiang, Q., Yang, J.: Frequency shifts in a quartz plate piezoelectric resonator in contact with a viscous fluid under a separated electrode. Int. J. Appl. Electromagnet. Mech. **35**, 177–187 (2011)
12. Du, J., Xian, K., Wang, J., Yang, J.: Thickness vibration of piezoelectric plates of 6 mm crystals with tilted six-fold axis and two-layered thick electrodes. Ultrasonics **49**, 149–152 (2009)
13. Vig, J.R., Ballato, A.: Comments on the effects of nonuniform mass loading on a quartz crystal microbalance. IEEE Trans. Ultrason. Ferroelectr. Freq. Control **45**, 1123–1124 (1998)
14. Yang, J.: Frequency shifts in a piezoelectric body due to small amounts of additional mass on its surface. IEEE Trans. Ultrason. Ferroelectr. Freq. Control **51**, 1199–1202 (2004)
15. Yang, J., Guo, S.: Vibrations of a crystal body with a shear-deformable surface mass layer. Acta Mech. **190**, 223–232 (2007)
16. Liu, N., Yang, J., Chen, W.: Effects of a mass layer with gradually varying thickness on a quartz crystal microbalance. IEEE Sens. J. **11**, 1635–1639 (2011)
17. Tiersten, H.F., Lwo, B.J., Dulmet, B.: Transversely varying thickness modes in trapped energy resonators with shallow and beveled contours. J. Appl. Phys. **80**, 1037–1046 (1996)
18. Wang, J., Shen, L., Yang, J.: Effects of electrodes with continuously varying thickness on energy trapping in thickness-shear mode quartz resonators. Ultrasonics **48**, 150–154 (2008)
19. Liu, N., Yang, J., Chen, W.: Effects of mass layer nonuniformity on a quartz-crystal microbalance. IEEE Sens. J. **11**, 934–938 (2011)
20. Mindlin, R.D.: Bechmann's number for harmonic overtones of thickness/twist vibrations of rotated Y-cut quartz plates. J. Acoust. Soc. Am. **41**, 969–973 (1967)
21. He, H., Liu, J., Yang, J.: Analysis of a monolithic crystal plate acoustic wave filter. Ultrasonics **51**, 991–996 (2011)
22. Joshi, S.P.: Non-linear constitutive relations for piezoceramic materials. Smart Mater. Struct. **1**, 80–83 (1992)

23. Tiersten, H.F.: Linear Piezoelectric Plate Vibrations. Plenum, New York (1969)
24. Kong, Y., Liu, J., He, H., Yang, J.: Effects of mass layer dimension on a finite quartz crystal microbalance. Acta Mech. **222**, 103–113 (2011)
25. Yang, J., Chen, Z., Hu, H.: Electrically forced vibration of a thickness-twist mode piezoelectric resonator with non-uniform electrodes. Acta Mech. Solida Sin. **20**, 266–274 (2007)
26. Yang, J., Chen, Z., Hu, Y.: Vibration of a thickness-twist mode piezoelectric resonator with asymmetric non-uniform electrodes. IEEE Trans. Ultrason. Ferroelectr. Freq. Control **55**, 841–848 (2008)
27. Bovik, P.: A comparison between the Tiersten model and O(H) boundary conditions for elastic surface waves guided by thin layers. ASME J. Appl. Mech. **63**, 162–167 (1996)
28. Chen, Y., Du, J., Wang, J., Yang, J.: Shear-horizontal waves in a rotated Y-cut quartz plate with an imperfectly bonded mass layer. IEEE Trans. Ultrason. Ferroelectr. Freq. Control **58**, 616–622 (2011)
29. Abdalla, A.N., Alsheikh, F., AlHossain, A.Y.: Effect of initial stresses on dispersion relation of transverse waves in a piezoelectric layered cylinder. Mat. Sci. Eng. B-Solod. **162**, 147–154 (2009)